Environmental Science and Pollution Research (2018) 25:25315–25326
https://doi.org/10.1007/s11356-018-2615-9

RESEARCH ARTICLE

Preparation and characterization of PSF/PEI/$CaCO_3$ nanocomposite membranes for oil/water separation

Seda Saki[1] · Nigmet Uzal[2]

Received: 1 February 2018 / Accepted: 18 June 2018 / Published online: 26 June 2018

Abstract

Ultrafiltration (UF) is one of the significant advanced processes for oily wastewater treatment due to its clear advantages, for instance, ease in operation and efficient separation. The main drawback of these processes is the fouling problem and many researchers' effort on fabrication of high-performance membranes with higher hydrophilicity and antifouling properties. In this study, flat-sheet polysulfone (PSF)/polyethylenimine (PEI)/$CaCO_3$ nanocomposite membranes were prepared by phase inversion method for oil/water emulsion separation. Structural properties of membranes were characterized by SEM, FT-IR, contact angle, tensile strength, and atomic force microscopy analysis. Increasing the $CaCO_3$ nanoparticle loading exhibited the increased the water flux and BSA rejection. PSF/PEI/10 wt% $CaCO_3$ nanocomposite membranes have 145 L/m^2 h water flux at 2 bar with a contact angle of 84° and with 92% BSA rejection. All prepared $CaCO_3$ nanocomposite membranes reached similar oil rejections at above 90%. Besides the higher water flux and oil removal efficiencies, 10 wt% of $CaCO_3$ nanoparticle-blended PSF membranes has notable antifouling capacity with the highest flux recovery ratio (FRR) and lowest flux decay ratio (DR) values. The results showed that there is a great potential to use PSF/PEI/$CaCO_3$ nanocomposite membranes for the treatment of oil water emulsions with higher permeability and antifouling capacity.

Keywords $CaCO_3$ nanoparticles · Nanocomposite membrane · Oil rejection · Antifouling

Introduction

Industrial wastewaters containing high oil should be treated before discharging through receiving environments due to its serious environmental problems (Ibrahim et al. 2001; Shi et al. 2016). In the treatment of oily wastewaters, application of conventional physicochemical treatment methods is limited due to low separation efficiencies, high energy consumption, and operating costs (Lin et al. 2012; Tummons et al. 2016). In recent years, ultrafiltration (UF) has been used commonly for purification of oily water due to low energy requirements, continuous operation, and higher removal efficiencies (Chang et al. 2001; Gryta et al. 2001; Kasemset et al. 2017). Nevertheless, membrane fouling is the major problem of membrane processes and, to overcome these problems, special membranes can be designed and prepared with polymeric materials and inorganic nanoparticles to enhance oil separation performance (Jhaveri and Murthy 2016; Li et al. 2006).

Polysulfone (PSF) is a popular membrane polymer for its use in water and wastewater treatments due to its mechanical robustness, structural and chemical stability, and thermal resistance (Yang et al. 2007; Yu et al. 2009). Besides the advantages of PSF, it needs to be modified to reduce its hydrophobic characteristics and increase its permeability, porosity, and antifouling capacity for treating wastewaters (Fenu et al. 2010; Kumar et al. 2013; Li and Chu 2003; van Reis and Zydney 2007). Thus, hydrophilic polymers (polyvinyl pyrrolidone, polyethylene glycol, polyvinyl alcohol) can be blended in the membrane matrix to create micropores and increase hydrophilicity (Zhao et al. 2011a). Polyethylenimine (PEI) is shown to be an attractive macrovoid formation agent with special

Responsible editor: Angeles Blanco

✉ Nigmet Uzal
nigmet.uzal@agu.edu.tr

[1] Materials Science and Mechanical Engineering, Abdullah Gül University, 38080 Kayseri, Turkey

[2] Department of Civil Engineering, Abdullah Gül University, 38080 Kayseri, Turkey

functions in terms of biocompatibility, chemical reactivity, and hydrophilicity (Park et al. 2012; Wu et al. 2014). However, the addition of hydrophilic polymers, including PEI, can decrease the mechanical strength, stability, and selectivity of the membrane (Ba et al. 2009). To overcome these problems in membranes, blending the polymer with inorganic nanoparticles offers several advantages, like higher selectivity, maintaining high permeate flux, and thermal and mechanical resistance (Abdullah et al. 2016) as in order to optimize the membrane performance (Ng et al. 2013).

Yang et al. (2007) showed that TiO_2 nanomaterial-blended PSF nanocomposite membranes gave better membrane properties in terms of water permeate flux, hydrophilicity, as well as mechanical strength and fouling resistance (Yang et al. 2007). Yi et al. (2011) fabricated PVDF UF membrane incorporated with nanosized TiO_2/Al_2O_3 to improve the antifouling resistance. Their results showed that TiO_2/Al_2O_3 addition provides better antifouling capacity and hydrophilicity and also desirable flux recovery has been obtained (Yi et al. 2011). In another study, Zhang et al. (2013) used PSF membranes with phosphorylated TiO_2–SiO_2 (PTS) particles for oily wastewater treatment. PTS particles improved the PSF membrane hydrophilicity, antifouling capacity, and mechanical strength significantly. The contact angle of the 10 wt% PTS embedded membrane decreased from 78.0° to 45.5° with 92% oil rejection and 116 L/m^2 h flux value at 0.1 MPa (Zhang et al. 2013). Similarly, Zhang et al. (2011) conducted a study for the enhancement of the hydrophilicity and antifouling capability of PSF membranes assisted with sulfonated zirconia particles (SZP) for treating oily wastewater. Experiments showed that the oil concentration in permeate decreased from 80 to 0.67 mg/L for 15 wt% SZP/PSF membrane with satisfied recycling standards (Zhang et al. 2011).

$CaCO_3$ nanoparticles have been attracted considerable attention in water and wastewater treatments because of its larger specific surface, great biocompatibility, and low cost (Shan et al. 2007). Additionally, $CaCO_3$ surface properties can improve water permeation due to its carboxylic groups and surface polarities (Wang et al. 2008). Within this context, PSF/PEI/$CaCO_3$ nanocomposite membranes were prepared via phase inversion process with PEI and $CaCO_3$ nanoparticle additives to increase flux and hydrophilicity of membranes and to improve their performance for oily water treatment. $CaCO_3$ nanoparticles were used in membrane matrix with different weight percentages of 1, 2, 5, and 10 wt%. The effect of concentration of $CaCO_3$ nanoparticles on the structural properties and filtration performance of the membranes was also investigated. To the best of our knowledge, there are no reported data involving PSF/PEI/$CaCO_3$-blended substrate to fabricate polymeric nanocomposite membranes for oily water treatment. The findings herein provide new insight on the role of PSF/PEI/$CaCO_3$ nanocomposite membranes in oil/water separation, which may contribute for the development of better nanocomposite membranes for water based filtration applications.

Experimental

Materials

PSF (average molecular weight of 60,000) was purchased from Acros Organics. An aqueous solution of branched PEI with a weight-average molecular weight of 25,000 was obtained from Sigma-Aldrich and used as a pore former. Dimethylformamide (DMF; Merck, anhydrous, 99.8%) and *N*-methyl-2-pyrrolidone (NMP; Merck) were used as solvents. Hydrophilic $CaCO_3$ nanoparticles with 100 nm were supplied from Nanografi, Turkey, and used as additives for the PSF/PEI solutions. Bovine serum albumin (BSA) was used as a foulant and supplied from Amresco Inc. (USA). Sodium dodecylsulfate (SDS) salt was used an emulsifier to encourage the suspension of water and oil phases and was purchased from SERVA Electrophoresis GmbH, Germany. Vacuum pump oil (G-19) was purchased from Edwards (UK). Ethanol was purchased from Merck. All of the organic and inorganic reagents were analytical grade.

Preparation of membranes

Commercial nanoparticles of $CaCO_3$ (100 nm) were first dissolved in NMP solution at four different concentrations of 1, 2, 5, and 10 wt%. The mixture was then sonicated for 2 h. Next, the $CaCO_3$ nanoparticles were dissolved with 20 wt% PSF and 2 wt% PEI in DMF and NMP mixture in a ratio of 7:3 (*w*/*w*) to form membrane casting solutions. The final solution was then mixed for 24 h at

Table 1 Casting solution compositions of PSF/PEI/$CaCO_3$ nanocomposite membranes

Membrane	PSF (wt%)	PEI (wt%)	$CaCO_3$ (wt%)
PSF	20	0	0
PSF/PEI	20	2	0
1 wt% $CaCO_3$	20	2	1
2 wt% $CaCO_3$	20	2	2
5 wt% $CaCO_3$	20	2	5
10 wt% $CaCO_3$	20	2	10

400 rpm using a magnetic stirrer to make the solution homogeneous. The polymer suspension was then sonicated for at least 2 h. The composition of the casting solutions is shown in Table 1.

Membrane characterization

Structural properties of membranes were characterized by scanning electron microscopy (SEM), Fourier transform infrared spectroscopy (FT-IR), porosity, viscosity, contact angle, tensile strength, and atomic force microscopy (AFM). The filtration performances were evaluated by measuring water flux, BSA, and oil rejection.

Viscosity measurements

The average viscosity of the dope solution was measured with a Rapid Visco Analyzer (Pertem, RVA 4500). The viscosity was determined at 25 ± 5 °C. To ensure the complete uniformity of the samples to be analyzed, the rotation of the RVA was set to 60 rpm for 120 s.

SEM

SEM affords the optical information of the membrane morphology in terms of pore structure, distribution, and density. The top-surface and cross-section morphologies of the membranes were observed using a Zeiss Evo LS10 scanning electron microscope. The membranes were carefully sectioned with an average 0.5 mm width and 3 mm length and then mounted onto the SEM grid. Before the analysis, each sample was coated with platinum, and the samples were analyzed at 10 kV.

Membrane hydrophilicity

Membrane surface hydrophilicity was quantified by measuring contact angle meter (Attention-Theta Lite, Biolin Scientific, Finland) with sessile drop method. Three microliters of deionized (DI) water was used to compare the hydrophilicity of the pure PSF, PSF/PEI, and PSF/PEI/$CaCO_3$ membranes. For each measurement, at least three readings from different surface locations were taken, and the average values are reported with standard deviations. All of the membranes were fully dried before measuring the contact angle to avoid water interaction.

Porosity

For the porosity measurements, dry membranes were immersed in ethanol for 2 h, and the liquid on the surfaces of the membranes was removed using filter paper. The membrane porosity (ε) was calculated using Eq. 1 (Lohokare et al. 2011):

$$\varepsilon = \frac{(\omega_1 - \omega_2)/d\omega}{\frac{\omega_1 - \omega_2}{d\omega} + \omega_2/dp} \quad (1)$$

where ω_1 is the weight of the wet membrane (g), ω_2 the weight of the dry membrane (g), $d\omega$ is the density of ethanol (0.789 g/cm^3), and dp is the polymer density (1.24 g/cm^3).

FT-IR

The FT-IR spectroscopy is an easy method to determine of the relative amounts of different functional groups of polymeric membranes with time resolution down to nanoseconds. FT-IR spectra were employed for identification of PEI and $CaCO_3$ nanoparticles using an FT-IR spectrometer (Thermo Nicolet Avatar 370). Prior to the FT-IR measurements, the samples were dried in a drying oven for 15 min at 120 °C.

Mechanical strength

The mechanical strength of the prepared membranes was measured using an AGS-J tensile testing machine (Shimadzu, Japan). The measurements were carried out according to the ASTM D 882 standard by applying a 500-N load at a crosshead speed of 1 mm/min. All the samples were sectioned with dimensions of 6 × 2 cm^2. The sample thicknesses were measured with an electronic micrometer with ± 0.1 μm precision (no. 293-561, Mitutoyo, Japan).

AFM analysis

Atomic force microscopy was used to determine the surface morphology and surface roughness (average surface roughness (R_a), root mean square roughness (R_q), and maximum height of the profile (R_{max})) of the prepared membranes at nanoscale. Membrane surface roughness was characterized by MultiMode 8-HR, Veeco operated in tapping mode (Model: RTESP-300). The membranes were dried overnight at 80 °C to evaporate the liquid completely from the membrane surfaces and pores. The analysis was performed using a 5-μm × 5-μm image size and a 3.4-Hz scan rate. The roughness parameters of each membrane were reported as the average of at least three measurements on membranes.

Water filtration tests

A dead-end stirred cell filtration system (Sterlitech, HP4750) was used to determine the membranes' intrinsic separation properties (i.e., water flux and rejection). Filtration cell

connected with a nitrogen gas cylinder and consisted of a filtration cell with a volume of 300 mL. The effective membrane area for the system was 14.6 cm^2. DI water was used as a feed solution for filtration test, and the feed side of the system was pressurized by nitrogen gas. In the water filtration test, transmembrane pressure (TMP) was at 2 bar for PSF, PSF/PEI, and PSF/PEI/$CaCO_3$ membranes, stirring speed was at 300 rpm, and the temperature was kept at 25 ± 5 °C. The water fluxes of the prepared membranes were calculated using Eq. 2:

$$J = \frac{V}{A \times \Delta t} \tag{2}$$

where J is the water flux (L/m^2 h), V is the permeate volume (L), A is the effective membrane area (m^2), and Δt is time (h). Oil/water emulsion refilled the stirred cell reservoir.

BSA rejection experiments The membranes' BSA rejection performance was determined using aqueous solutions containing 2.5 g/L of BSA at 2 bar TMP in the dead-end filtration module (Jamal et al. 2014). The solutions were prepared using DI water at room temperature. BSA concentrations were analyzed using UV–visible spectroscopy at a wavelength of 280 nm. The BSA rejections (R) were calculated by Eq. 3:

$$\%R = 1 - \frac{C_p}{C_f} \times 100 \tag{3}$$

where C_p is the concentration of BSA in the permeate, and C_f is the concentration of BSA in the feed solution. The volume reduction ratio (VRR) is calculated using the following Eq. 4:

$$\mathrm{VRR} = \frac{V_0}{V_R} \tag{4}$$

where V_0 and V_R are the initial feed volume and retentate volume, respectively.

Oil rejection experiments The vacuum pump oil (G-19) was used for preparation synthetic oil/water emulsion. The oil rejection tests were conducted at 300 rpm stirring speed and at 2 bar TMP in the dead-end filtration module. The emulsion was prepared with mixing of oil and surfactant SDS in a ratio of 9:1 (w/w) and 500 mL DI water. The emulsion was mixed for 30 min and stored at room temperature.

After the clean membrane pure water flux (J) was calculated, solution reservoir was filled with oil/water emulsion and oil/water emulsion flux (J_1) was calculated by using Eq. 2. After filtration of oil/water emulsion, solution reservoir was emptied and the membranes were cleaned with DI water for 20 min and refilled with the DI water; cleaned membrane water flux (J_2) was calculated in the similar with Eq. 2. Oil concentration of wastewater samples were analyzed using UV–visible spectroscopy at a wavelength of 283 nm.

The oil rejections (R) and VRR were calculated using Eqs. 3 and 4.

Fouling resistance was evaluated using oil/water emulsion flux decay ratio (DR) (Geng et al. 2017) and flux recovery ratio (FRR) (Chen et al. 2009; Zhao et al. 2011b) and calculated using the following equations (Eqs. 5 and 6):

$$\mathrm{DR} = \frac{J - J_1}{J} \times 100 \tag{5}$$

$$\mathrm{FRR} = \frac{J_2}{J} \times 100 \tag{6}$$

where J (L/m^2 h) is the water flux before fouling, J_1 (L/m^2 h) is the oil/water emulsion flux, and J_2 (L/m^2 h) cleaned membrane water flux.

Results and discussions

Membrane morphology

Viscosity of membrane dope solutions

Viscosity is one of the most important parameter for the membrane fabrication because it affects the solvent–non-solvent exchange rate and so the final morphology of formed membranes (Alpatova et al. 2013). PSF/PEI and PSF/PEI/$CaCO_3$ nanocomposite membranes viscosity values are shown in Fig. 1. The viscosity values of casting solutions were increased significantly with increasing $CaCO_3$ nanoparticles loading because of higher shear stress. As shown in Fig. 1, increasing the $CaCO_3$ concentration from 1 to 10 wt% increased the viscosity from 680 to 2530 cp. The highest viscosity was obtained for the PSF/PEI/$CaCO_3$ solution containing 10 wt% $CaCO_3$ nanoparticles. This result can be explained in terms of the adsorption between the polymeric chains and the exposed hydroxyl groups at the surface of the nanoparticles, which have high specific surface area and surface energy (Aerts et al. 2000; Yang et al. 2007). Nair et al. (2013) also showed that the addition of $CaCO_3$ nanoparticles in PSF membrane increases the viscosity values (Nair et al. 2013). In another study showed that the addition of $CaCO_3$ nanoparticles in isotactic polypropylene matrix was responsible for increasing the shear viscosity of dope solution with increasing $CaCO_3$ content (Dangtungee et al. 2005).

SEM images

Top and cross-section structures of prepared PSF/PEI/$CaCO_3$ nanocomposite membranes were investigated by SEM to provide a better insight for the characterization and development

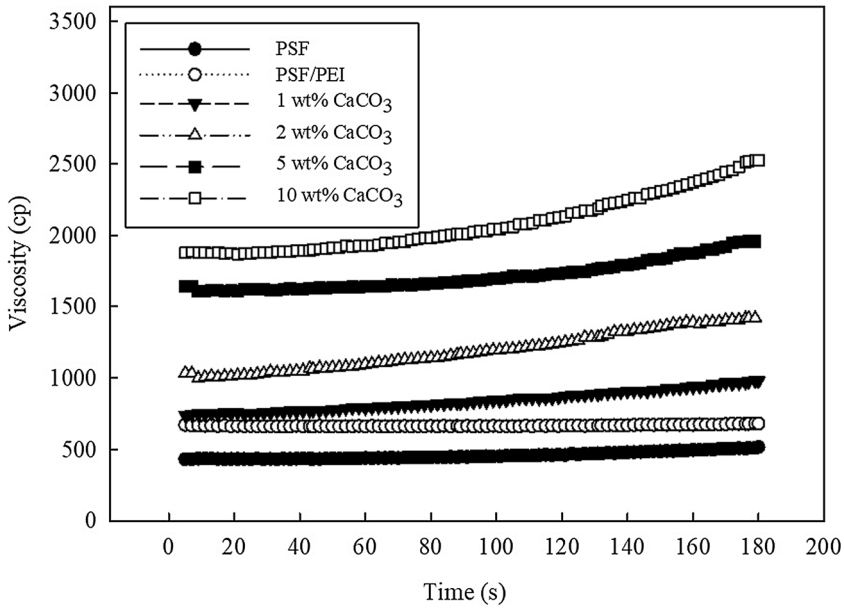

Fig. 1 The casting solution viscosity values of PSF, PSF/PEI, and PSF/PEI/$CaCO_3$ nanocomposite membranes

of membranes. Figure 2 shows top surface images of 20 wt% PSF and PSF/PEI membrane with 2 wt% PEI addition to the polymer matrix. However, 20 wt% PSF has uniform surface without nodules and the surface pore structure was completely changed and had small pores when 2 wt% PEI was added to the polymer matrix.

Surface images of the PSF/PEI membranes with different concentrations of $CaCO_3$ (1, 2, 5, 10 wt%) are shown in Fig. 3. As shown in Fig. 3, although the concentration of $CaCO_3$ nanoparticles was high, agglomeration problem was not observed. Chan et al. (2002) also reported similar results when $CaCO_3$ content was lower than 20 wt% in membrane matrix. However, over 20 wt% $CaCO_3$ loading aggregation on membrane surface was reported (Chan et al. 2002). Besides no aggregation, the increased $CaCO_3$ nanoparticles result in the development of more porous structure on the PSF membrane surface.

Cross-section images of PSF/PEI/$CaCO_3$ nanocomposite membranes are given in Fig. 4. Cross-section structures of PSF/PEI/$CaCO_3$ nanocomposite membranes changed and new pore structures formed with $CaCO_3$ addition to the polymer matrix. Compared with Fig. 4a, d, the higher viscosity induces slower exchange between solvent and non-solvent for the formation of porous structure increasing with $CaCO_3$ concentration. The hydrophilic PEI and $CaCO_3$ content in membrane matrix should have resulted in fast exchange because of higher viscosity which resulted microporous membranes structure during the phase inversion (Chung et al. 2016). Another possibility can be the increasing concentration of $CaCO_3$ resulted in more porous structure, and this is resulted in a decrease in the mechanical and thermal resistance of the membrane solution (Vo et al. 2017).

Membrane hydrophilicity and pure water flux

Hydrophilicity of PSF, PSF/PEI, and PSF/PEI/$CaCO_3$ nanocomposite membranes was determined and is given in Table 2. The increase of $CaCO_3$ in membrane matrix decreased the contact angle values from 92° to 80° for pure PSF membrane and for PSF/PEI/$CaCO_3$ (5 wt% $CaCO_3$), respectively. This

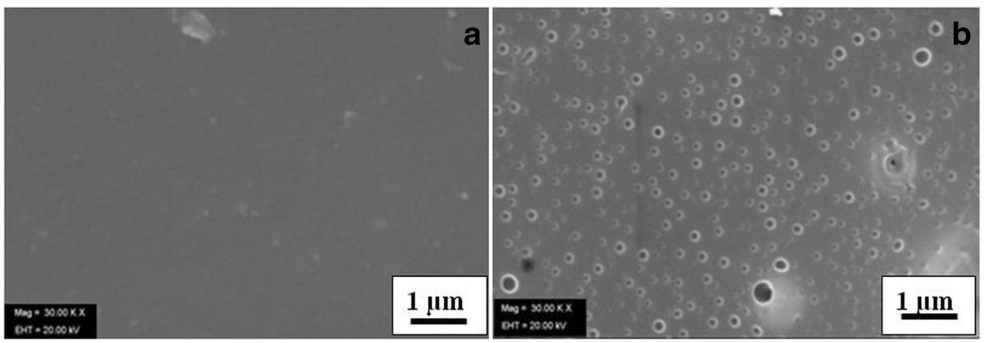

Fig. 2 SEM surface images of 20 wt% PSF membranes containing different concentrations of PEI. **a** 0 wt%. **b** 2 wt%

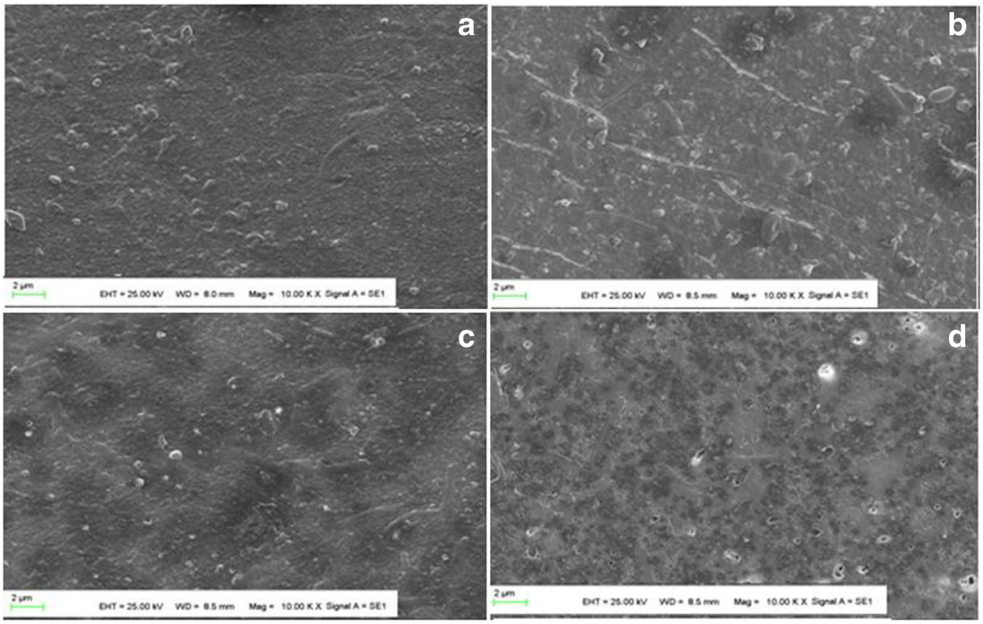

Fig. 3 Surface SEM images of PSF/PEI membrane containing different concentrations of $CaCO_3$ nanoparticles. **a** 1 wt%. **b** 2 wt%. **c** 5 wt%. **d** 10 wt%

hydrophilicity improvement can be attributed to the formation of OH groups which formed due to hydroxylation on the membrane surface (Cui et al. 2008).

The pure PSF membrane showed the lowest water flux of 3.1 L/m^2 h, and the highest water flux was obtained for the membranes with 10 wt% $CaCO_3$ nanoparticles as 145 L/m^2 h. PSF/PEI/10 wt% $CaCO_3$ nanocomposite membrane pure water flux improved over 50 times higher than pure PSF membrane. This result could be explained by the improvement of the hydrophilicity and porosity of PSF/PEI/$CaCO_3$ membranes by addition of $CaCO_3$ (Celik et al. 2011; Kim et al. 2012). According to the results given in Table 2, although the contact angle values were slightly decreased with addition of $CaCO_3$ nanoparticles, water flux values were enhanced with the increase in $CaCO_3$ loading.

Porosity

Membrane porosity is generally dependent on the mass transfer of the casting solution during the phase inversion process (Hong and He 2014) and solvent and non-solvent exchange rate. $CaCO_3$ could be easily dispersed with different weight ratios in membrane structure and very promising alternative nanoparticle for water treatment (Abebe et al. 2015; Yu et al.

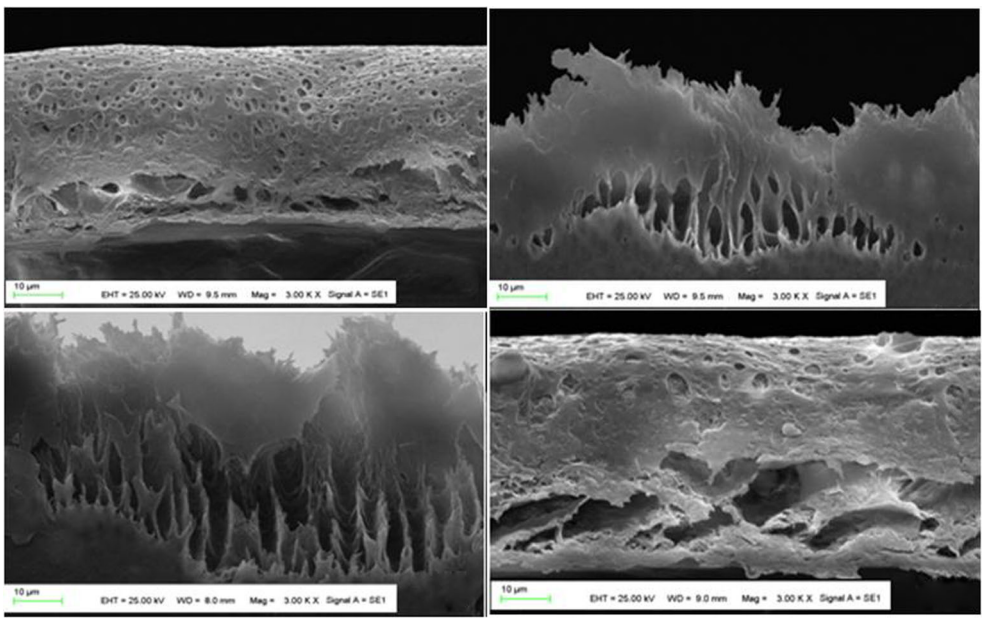

Fig. 4 Cross-section SEM images of PSF/PEI membrane containing different concentrations of $CaCO_3$ nanoparticles. **a** 1 wt%. **b** 2 wt%. **c** 5 wt%. **d** 10 wt%

Table 2 Contact angle, pure water flux (2 bar), and porosity of PSF, PSF/PEI, and PSF/PEI/$CaCO_3$ nanocomposite membranes

Substrate	CA (°)	Water flux (L/m^2 h)	Porosity (%)
PSF	92 ± 5	3.1 ± 0.2	27 ± 3
PSF/PEI	85 ± 4	180 ± 13	58 ± 5
1 wt% $CaCO_3$	87 ± 7	45 ± 12	74 ± 8
2 wt% $CaCO_3$	86 ± 5	48.7 ± 8	76 ± 3
5 wt% $CaCO_3$	80 ± 6	48 ± 26	75 ± 6
10 wt% $CaCO_3$	84 ± 8	145 ± 21	70 ± 2

2013). It can be seen that in Table 2, porosity values were significantly increased with $CaCO_3$ loading when compared to the PSF and PSF/PEI membranes. PSF and PSF/PEI dense structure causes the lowest porosity with 27 and 58%, respectively. All PSF/PEI/$CaCO_3$ nanocomposite membranes have similar porosity values, and the maximum porosity was observed as 76% for PSF/PEI/$CaCO_3$ membrane with 2 wt% of $CaCO_3$ content. The interaction between the polymer and the solvent molecules declined by the obstruction of nanoparticles and resulted in more and easy diffusion of solvent molecules from the polymer matrix to the coagulation bath. Besides this, with the addition of $CaCO_3$, the total solid content was increased and the porosity was decreased (Vatanpour et al. 2012).

Mechanical properties

Hydrophilic $CaCO_3$ addition in polymer matrix could enhance the membrane morphology as well as mechanical properties especially tensile strength. In the evaluation of UF membranes for the practical applications, the mechanical strength of the membranes is the key factor (Xu et al. 2014). The mechanical properties of the polymeric materials can be developed significantly with nanoparticle addition because of improvement of the compatibility between the filler and polymer (Chan et al. 2002). $CaCO_3$ has been used as an important nanofiller in polymeric materials (Osman et al. 2004). Figure 5 illustrates strain–stress curve of PSF and PSF/PEI/$CaCO_3$ membranes. According to the results, tensile stress increased with $CaCO_3$ addition. The tensile strength of pure PSF was 4.1 MPa, and the tensile strength was increased to 7.8 MPa when the $CaCO_3$ content is increased to 10 wt%.

FT-IR

The surface chemical compositions of PSF/PEI/$CaCO_3$ nanocomposite membranes were determined by FT-IR spectroscopy and are shown in Fig. 6. The PSF characteristic peaks were around 1149 and 1168 cm^{-1} (SO_2 symmetrical stretching), 1244 cm^{-1} (aryl-O-aryl C–O stretching), 1582 cm^{-1} (SO_2 asymmetric stretching), 1677 cm^{-1} (asymmetric–CH_3), and 2151 cm^{-1} (C=C) (Dehghani Kiadehi et al. 2015; Rupiasih et al. 2013). All prepared nanocomposite membranes showed a band at 2969 cm^{-1} which is corresponding to CH_2 stretching (Kurapati and Raichur 2013) and it is caused by the main polymer (PSF) in membrane matrix. After $CaCO_3$ addition, the characteristic vibration peaks of $CaCO_3$ were obtained at the peak intensities of 704, 871, and 1408 cm^{-1} (Zhi et al. 2014). The –OH bending vibrations of $CaCO_3$ nanoparticles were attributed at 1650 cm^{-1} (Abdolmohammadi et al. 2012). At the same time, a shoulder

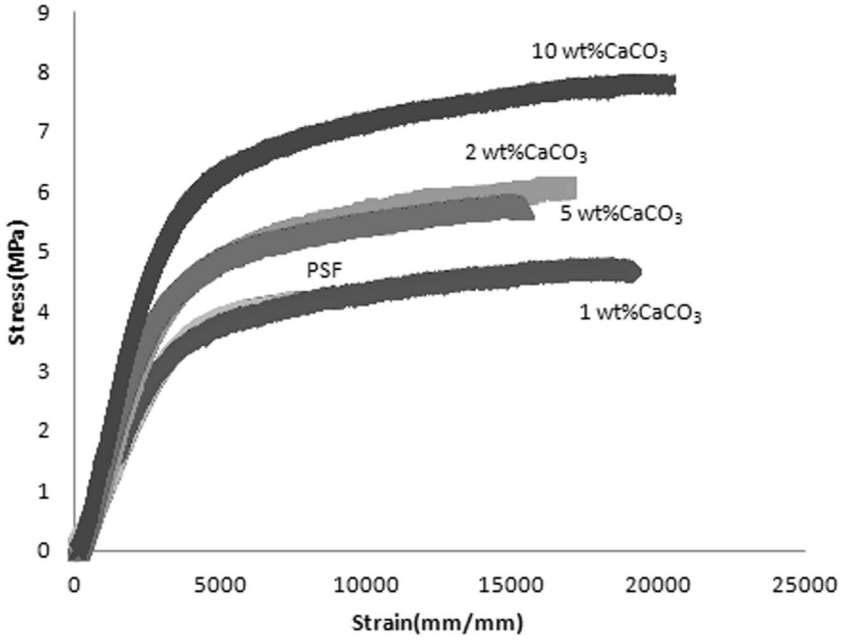

Fig. 5 Strain–stress curve of PSF and PSF/PEI/$CaCO_3$ membranes

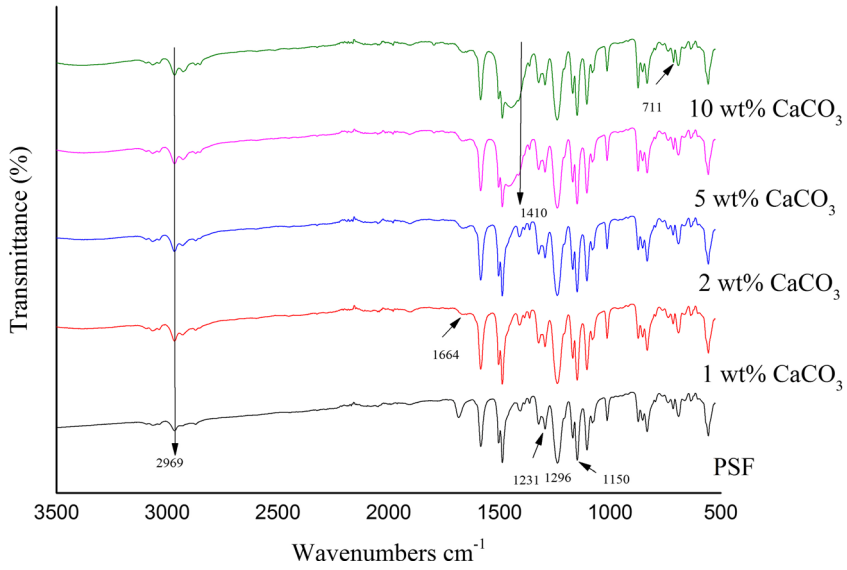

Fig. 6 FT-IR spectrum of PSF and PSF/PEI/$CaCO_3$ nanocomposite membranes

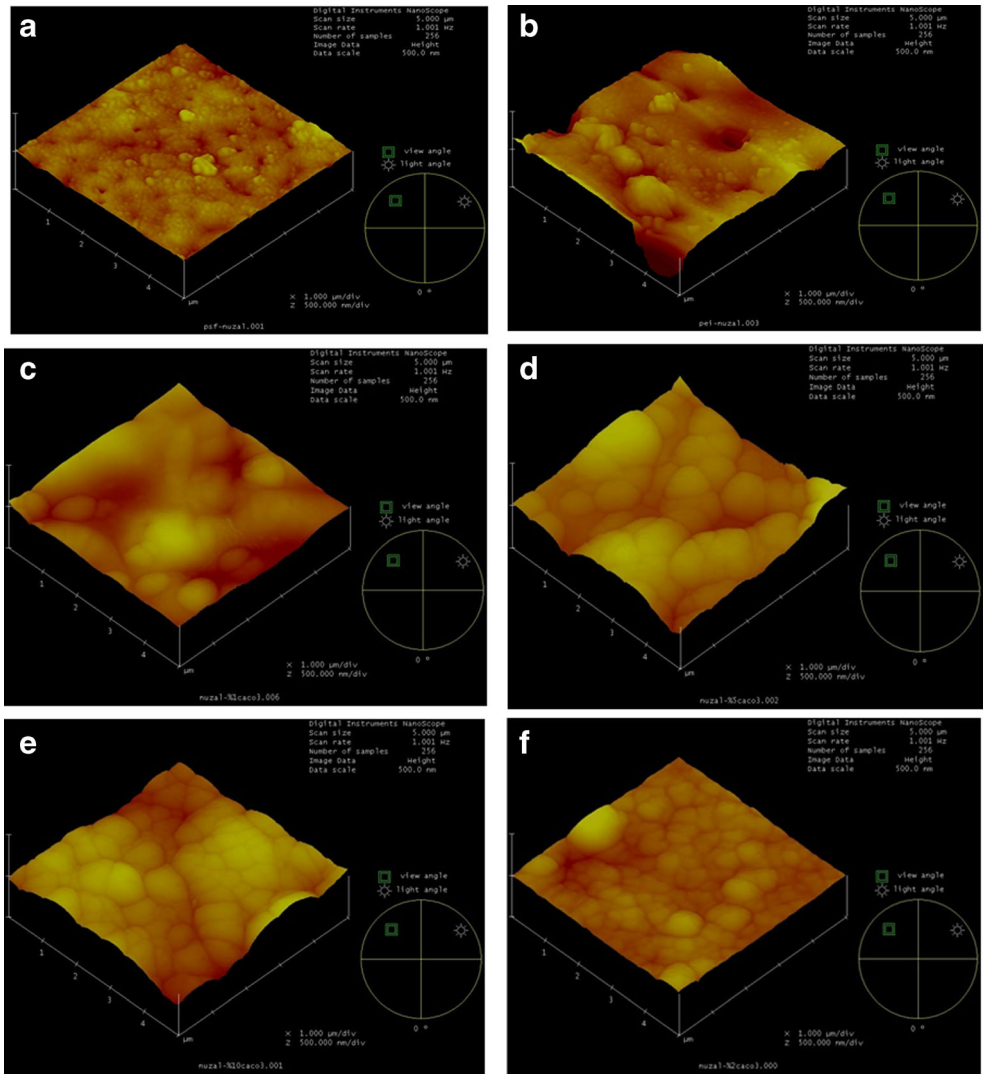

Fig. 7 AFM images of **a** PSF, **b** PSF/PEI, and PSF/PEI/$CaCO_3$ nanocomposite membranes containing $CaCO_3$ nanoparticles. **c** 1 wt%. **d** 2 wt%. **e** 5 wt%. **f** 10 wt%

peak was obtained near 1408 cm^{-1} which corresponds the amorphous structure of $CaCO_3$. In addition, the peak at 1664 cm^{-1} is assigned to the vibration of water molecules bounded on the $CaCO_3$ particles (Hou et al. 2014; Lam et al. 2007; Zhi et al. 2014). As seen in Fig. 6, the merged peaks became more obvious with the increase in concentration of $CaCO_3$ from 5 to 10 wt% and this is the evidence of the successful linkage of $CaCO_3$ in PSF.

AFM

The three-dimensional images of AFM analysis are shown in Fig. 7 and clearly observed from AFM images that PSF membrane smoother structure changed significantly with the addition of $CaCO_3$ nanoparticles.

The roughness parameters, R_q, R_a, and R_{max}, are given in Table 3. The surface roughness of the PSF/PEI/$CaCO_3$ nanocomposite membranes was apparently higher than that of the pure PSF membrane. Zhang et al. (2013) reported that the membrane with high surface roughness increases surface area and causes cavities, both promoting permeation. This could be due to the contaminants accumulating on the membranes surface resulted as a rough surface and permeation was increased. Thus, increase in membrane-surface roughness does not have a negative effect on membrane performance. PSF/PEI membrane showed higher R_a value than PSF/PEI/1 wt% $CaCO_3$ and PSF/PEI/2 wt% $CaCO_3$ membranes, and Khayet (2004) explain that higher solvent evaporation time of PEI during phase inversion process (Khayet 2004).

BSA rejection

The BSA flux and BSA rejection values of prepared PSF, PSF/PEI, and PSF/PEI/$CaCO_3$ membranes are given in Table 4. The BSA rejection values of the pure PSF and PSF/PEI membranes were 94 and 97%, respectively. It is observed that all of the prepared membranes rejected more than 90% of the BSA, and PSF/PEI/2 wt% $CaCO_3$ nanocomposite membrane showed the highest BSA rejection with 98%. According to the results, PSF/PEI/$CaCO_3$ nanocomposite membranes showed UF characteristics due to over 90% BSA rejection ratios (Yan et al. 2005).

Oil rejection

To evaluate the oil rejection performance of PSF/PEI/$CaCO_3$ nanocomposite membranes, synthetic vacuum oily solution (1000 ppm) was used in experiments. Although PSF membranes showed the lowest oil rejection ratio with 88%, all PSF/PEI/$CaCO_3$ nanocomposite membranes rejected oil over 99%. The oil water fluxes decreased with time due to the accumulation on the membrane surface, which shows that water mass transfer was limited. In the serial filtration operation, the deposition and re-suspension of oil reached equilibrium on the membrane surface, so that a stable flux was obtained. The stable oil/emulsion fluxes for PSF/PEI/$CaCO_3$ nanocomposite membranes were 28, 26, 32, and 98 L/m^2 h at 2 bar for the membranes with 1, 2, 5, and 10 wt% $CaCO_3$ nanoparticles loading, respectively.

Figure 8 shows the pure water flux measurements before and after synthetic oily water filtration and oily water fluxes of PSF, PSF/PEI, and PSF/PEI/$CaCO_3$ membranes. The oily water flux decreased considerably in comparison with pure water flux. This flux decline widely resulted in membrane fouling. Oil droplets adsorption and deposition on the membrane surface was built up rapidly, and membrane fouling was occurred directly. Membranes were cleaned for 20 min with pure water. After that, flux recovery was calculated to express the antifouling resistance of the membranes with FRR (Teli et al. 2012; Yan et al. 2005).

Oil rejection, FRR, and DR values of PSF, PSF/PEI, and PSF/PEI/$CaCO_3$ membranes are given in Table 5. According to the results; all PSF/PEI/$CaCO_3$ nanocomposite membranes showed higher FRR values than pure PSF and PSF/PEI membranes. The maximum FRR of 100% was observed with 1 and 10 wt% of $CaCO_3$ nanoparticle incorporated PSF/PEI/$CaCO_3$ membranes. This could be explained by the hydroxylation of $CaCO_3$ nanoparticles on membrane surface with increasing the hydrophilicity and weakening the interactions between

Table 3 The roughness properties of PSF, PSF/PEI, and PSF/PEI/$CaCO_3$ nanocomposite membranes

Substrate	R_q (nm)	R_a (nm)	R_{max} (nm)
PSF	12	9	137
PSF/PEI	57	40	522
1 wt% $CaCO_3$	35	25	316
2 wt% $CaCO_3$	24	18	153
5 wt% $CaCO_3$	44	32	308
10 wt% $CaCO_3$	59	48	386

Table 4 The BSA flux and rejection of PSF, PSF/PEI, and PSF/PEI/$CaCO_3$ nanocomposite membranes

Substrate	BSA flux[a] (L/m^2 h)	Rejection (%)
PSF	0.9	94
PSF/PEI	20.2	97
1 wt% $CaCO_3$	7.3	96
2 wt% $CaCO_3$	18.1	98
5 wt% $CaCO_3$	8.2	95
10 wt% $CaCO_3$	78	92

[a] The flux for BSA protein solution was measured at 2 bar

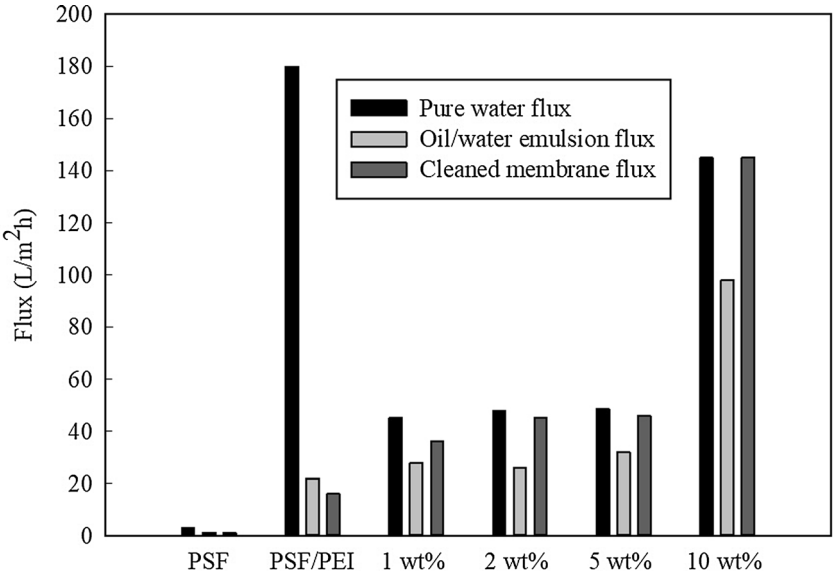

Fig. 8 Pure water, synthetic oily water, and cleaned membrane fluxes of PSF, PSF/PEI, and PSF/PEI/$CaCO_3$ membranes

oil and membrane surface (Cui et al. 2008). Ten weight percent of $CaCO_3$ nanoparticle membranes has notable antifouling capacity with the highest FRR and lowest DR values. Ahmad et al. (2011) fabricated PSF/SiO_2 nanocomposite membrane for oil/water emulsion separation and reported that increasing SiO_2 nanoparticle concentration from 1 to 3 g resulted as a decrease in DR values from 98 to 86% and increase in FRR values from 10 to 34% (Ahmad et al. 2011). In another study, although PSF/hydrous aluminum oxide (HAO) membrane eliminated all the oil molecules (100% rejection) with excellent permeation flux of 1194 L/m^2 hbar, the maximum FRR value was reported of 67% (Jamshidi Gohari et al. 2015). The results showed that $CaCO_3$ nanoparticles could be more effective for oil/water emulsion separation which improved not only oil rejection but also its antifouling capacity.

Conclusions

In this study, PSF/PEI/$CaCO_3$ nanocomposite membranes with improved separation and antifouling performance were developed for oily water treatment. Within this context, effect of hydrophilic and low-cost $CaCO_3$ nanoparticle on membrane structure and physicochemical properties were evaluated. According to the results of the experiments, the porosity, viscosity, water flux, and tensile strength of the PSF/PEI/$CaCO_3$ nanocomposite membranes were improved with the loading of $CaCO_3$ nanoparticles. Ten weight percent of $CaCO_3$ nanoparticle loading exhibited the highest water flux of 145 L/m^2 h at 2 bar with a contact angle of 84° and porosity of 70% with 92% BSA rejection. All $CaCO_3$ nanocomposite membranes reached similar oil rejections at over 90%. Besides this, PSF/PEI/$CaCO_3$ nanocomposite membranes with 10 wt% of $CaCO_3$ nanoparticles have notable antifouling capacity with the highest FRR and lowest DR values of 100 and 32%, respectively. These results have demonstrated that there is a great potential to use these PSF/PEI/$CaCO_3$ nanocomposite membranes in oily water treatment with higher permeability and antifouling capacity.

Table 5 Oil rejection ratio (%), FRR (%), and DR (%) values of PSF, PSF/PEI, and PSF/PEI/$CaCO_3$ membranes for synthetic oil/water emulsion filtration

Substrate	Oil rejection (%)	DR (%)	FRR (%)
PSF	88	61	32
PSF/PEI	99	87	48
1 wt% $CaCO_3$	> 99.9	37	82
2 wt% $CaCO_3$	> 99.9	46	94
5 wt% $CaCO_3$	> 99.9	33	95
10 wt% $CaCO_3$	> 99.9	32	100

References

Abdolmohammadi S, Siyamak S, Ibrahim NA, Yunus WMZW, Rahman MZA, Azizi S, Fatehi A (2012) Enhancement of mechanical and thermal properties of polycaprolactone/chitosan blend by calcium carbonate nanoparticles. Int J Mol Sci 13:4508–4522

Abdullah N, Gohari RJ, Yusof N, Ismail AF, Juhana J, Lau WJ, Matsuura T (2016) Polysulfone/hydrous ferric oxide ultrafiltration mixed matrix membrane: preparation, characterization and its adsorptive removal of lead (II) from aqueous solution. Chem Eng J 289:28–37

Abebe M, Hedin N, Bacsik Z (2015) Spherical and porous particles of calcium carbonate synthesized with food friendly polymer additives. Cryst Growth Des 15:3609–3616

Aerts P, Van Hoof E, Leysen R, Vankelecom IFJ, Jacobs PA (2000) Polysulfone–aerosil composite membranes: part 1. The influence

of the addition of aerosil on the formation process and membrane morphology. J Membr Sci 176:63–73

Ahmad A, Majid M, Ooi B (2011) Functionalized PSf/SiO2 nanocomposite membrane for oil-in-water emulsion separation. Desalination 268:266–269

Alpatova A, Kim E-S, Sun X, Hwang G, Liu Y, El-Din MG (2013) Fabrication of porous polymeric nanocomposite membranes with enhanced anti-fouling properties: effect of casting composition. J Membr Sci 444:449–460

Ba C, Langer J, Economy J (2009) Chemical modification of P84 copolyimide membranes by polyethylenimine for nanofiltration. J Membr Sci 327:49–58

Celik E, Liu L, Choi H (2011) Protein fouling behavior of carbon nanotube/polyethersulfone composite membranes during water filtration. Water Res 45:5287–5294

Chan C-M, Wu J, Li J-X, Cheung Y-K (2002) Polypropylene/calcium carbonate nanocomposites. Polymer 43:2981–2992

Chang I-S, Chung C-M, Han S-H (2001) Treatment of oily wastewater by ultrafiltration and ozone. Desalination 133:225–232

Chen W, Su Y, Zheng L, Wang L, Jiang Z (2009) The improved oil/water separation performance of cellulose acetate-graft-polyacrylonitrile membranes. J Membr Sci 337:98–105

Chung YT, Ba-Abbad MM, Mohammad AW, Benamor A (2016) Functionalization of zinc oxide (ZnO) nanoparticles and its effects on polysulfone-ZnO membranes. Desalin Water Treat 57:7801–7811

Cui ZG, Shi KZ, Cui YZ, Binks BP (2008) Double phase inversion of emulsions stabilized by a mixture of CaCO3 nanoparticles and sodium dodecyl sulphate. Colloids Surf A Physicochem Eng Asp 329:67–74

Dangtungee R, Yun J, Supaphol P (2005) Melt rheology and extrudate swell of calcium carbonate nanoparticle-filled isotactic polypropylene. Polym Test 24:2–11

Dehghani Kiadehi A, Rahimpour A, Jahanshahi M, Ghoreyshi AA (2015) Novel carbon nano-fibers (CNF)/polysulfone (PSf) mixed matrix membranes for gas separation. J Ind Eng Chem 22:199–207

Fenu A, Guglielmi G, Jimenez J, Spèrandio M, Saroj D, Lesjean B, Brepols C, Thoeye C, Nopens I (2010) Activated sludge model (ASM) based modelling of membrane bioreactor (MBR) processes: a critical review with special regard to MBR specificities. Water Res 44:4272–4294

Geng Z, Yang X, Boo C, Zhu S, Lu Y, Fan W, Huo M, Elimelech M, Yang X (2017) Self-cleaning anti-fouling hybrid ultrafiltration membranes via side chain grafting of poly(aryl ether sulfone) and titanium dioxide. J Membr Sci 529:1–10

Gryta M, Karakulski K, Morawski A (2001) Purification of oily wastewater by hybrid UF/MD. Water Res 35:3665–3669

Hong J, He Y (2014) Polyvinylidene fluoride ultrafiltration membrane blended with nano-ZnO particle for photo-catalysis self-cleaning. Desalination 332:67–75

Hou D, Dai G, Fan H, Wang J, Zhao C, Huang H (2014) Effects of calcium carbonate nano-particles on the properties of PVDF/nonwoven fabric flat-sheet composite membranes for direct contact membrane distillation. Desalination 347:25–33

Ibrahim M, Mostafa S, Fahmy M, Hafez A (2001) Utilization of electroflotation in remediation of oily wastewater. Sep Sci Technol 36:3749–3762

Jamal S, Chang S, Zhou H (2014) Filtration behaviour and fouling mechanisms of polysaccharides. Membranes 4:319–332

Jamshidi Gohari R, Korminouri F, Lau WJ, Ismail AF, Matsuura T, Chowdhury MNK, Halakoo E, Jamshidi Gohari MS (2015) A novel super-hydrophilic PSf/HAO nanocomposite ultrafiltration membrane for efficient separation of oil/water emulsion. Sep Purif Technol 150:13–20

Jhaveri JH, Murthy Z (2016) A comprehensive review on anti-fouling nanocomposite membranes for pressure driven membrane separation processes. Desalination 379:137–154

Kasemset S, Wang L, He Z, Miller DJ, Kirschner A, Freeman BD, Sharma MM (2017) Influence of polydopamine deposition conditions on hydraulic permeability, sieving coefficients, pore size and pore size distribution for a polysulfone ultrafiltration membrane. J Membr Sci 522:100–115

Khayet M (2004) Membrane surface modification and characterization by X-ray photoelectron spectroscopy, atomic force microscopy and contact angle measurements. Appl Surf Sci 238:269–272

Kim E-S, Hwang G, Gamal El-Din M, Liu Y (2012) Development of nanosilver and multi-walled carbon nanotubes thin-film nanocomposite membrane for enhanced water treatment. J Membr Sci 394-395:37–48

Kumar R, Isloor AM, Ismail AF, Rashid SA, Ahmed AA (2013) Permeation, antifouling and desalination performance of TiO2 nanotube incorporated PSf/CS blend membranes. Desalination 316:76–84

Kurapati R, Raichur AM (2013) Composite cyclodextrin-calcium carbonate porous microparticles and modified multilayer capsules: novel carriers for encapsulation of hydrophobic drugs. J Mater Chem B 1:3175–3184

Lam RS, Charnock JM, Lennie A, Meldrum FC (2007) Synthesis-dependant structural variations in amorphous calcium carbonate. CrystEngComm 9:1226–1236

Li X-y, Chu HP (2003) Membrane bioreactor for the drinking water treatment of polluted surface water supplies. Water Res 37:4781–4791

Li YS, Yan L, Xiang CB, Hong LJ (2006) Treatment of oily wastewater by organic–inorganic composite tubular ultrafiltration (UF) membranes. Desalination 196:76–83

Lin H, Gao W, Meng F, Liao B-Q, Leung K-T, Zhao L, Chen J, Hong H (2012) Membrane bioreactors for industrial wastewater treatment: a critical review. Crit Rev Environ Sci Technol 42:677–740

Lohokare H, Bhole Y, Taralkar S, Kharul U (2011) Poly(acrylonitrile) based ultrafiltration membranes: optimization of preparation parameters. Desalination 282:46–53

Nair AK, Isloor AM, Kumar R, Ismail AF (2013) Antifouling and performance enhancement of polysulfone ultrafiltration membranes using CaCO3 nanoparticles. Desalination 322:69–75

Ng LY, Mohammad AW, Leo CP, Hilal N (2013) Polymeric membranes incorporated with metal/metal oxide nanoparticles: a comprehensive review. Desalination 308:15–33

Osman MA, Atallah A, Suter UW (2004) Influence of excessive filler coating on the tensile properties of LDPE–calcium carbonate composites. Polymer 45:1177–1183

Park S-J, Cheedrala RK, Diallo MS, Kim C, Kim IS, Goddard WA (2012) Nanofiltration membranes based on polyvinylidene fluoride nanofibrous scaffolds and crosslinked polyethyleneimine networks. J Nanopart Res 14:884

Rupiasih NN, Suyanto H, Sumadiyasa M, Wendri N (2013) Study of effects of low doses UV radiation on microporous polysulfone membranes in sterilization process. Open J Org Polymer Mater 3:12–18

Shan D, Wang S, Xue H, Cosnier S (2007) Direct electrochemistry and electrocatalysis of hemoglobin entrapped in composite matrix based on chitosan and CaCO3 nanoparticles. Electrochem Commun 9:529–534

Shi H, He Y, Pan Y, Di H, Zeng G, Zhang L, Zhang C (2016) A modified mussel-inspired method to fabricate TiO2 decorated superhydrophilic PVDF membrane for oil/water separation. J Membr Sci 506:60–70

Teli SB, Molina S, Calvo EG, Lozano AE, de Abajo J (2012) Preparation, characterization and antifouling property of polyethersulfone–PANI/PMA ultrafiltration membranes. Desalination 299:113–122

Tummons EN, Tarabara VV, Chew Jia W, Fane AG (2016) Behavior of oil droplets at the membrane surface during crossflow microfiltration of oil–water emulsions. J Membr Sci 500:211–224

van Reis R, Zydney A (2007) Bioprocess membrane technology. J Membr Sci 297:16–50

Vatanpour V, Madaeni SS, Khataee AR, Salehi E, Zinadini S, Monfared HA (2012) TiO2 embedded mixed matrix PES nanocomposite membranes: influence of different sizes and types of nanoparticles on antifouling and performance. Desalination 292:19–29

Vo NT, Patra AK, Kim D (2017) Pore size and concentration effect of mesoporous silica nanoparticles on the coefficient of thermal expansion and optical transparency of poly(ether sulfone) films. Phys Chem Chem Phys 19:1937–1944

Wang L, Meng Z, Yu Y, Meng Q, Chen D (2008) Synthesis of hybrid linear-dendritic block copolymers with carboxylic functional groups for the biomimetic mineralization of calcium carbonate. Polymer 49: 1199–1210

Wu D, Huang Y, Yu S, Lawless D, Feng X (2014) Thin film composite nanofiltration membranes assembled layer-by-layer via interfacial polymerization from polyethylenimine and trimesoyl chloride. J Membr Sci 472:141–153

Xu Z, Zhang J, Shan M, Li Y, Li B, Niu J, Zhou B, Qian X (2014) Organosilane-functionalized graphene oxide for enhanced antifouling and mechanical properties of polyvinylidene fluoride ultrafiltration membranes. J Membr Sci 458:1–13

Yan L, Li YS, Xiang CB (2005) Preparation of poly(vinylidene fluoride)(pvdf) ultrafiltration membrane modified by nano-sized alumina (Al2O3) and its antifouling research. Polymer 46:7701–7706

Yang Y, Zhang H, Wang P, Zheng Q, Li J (2007) The influence of nano-sized TiO2 fillers on the morphologies and properties of PSF UF membrane. J Membr Sci 288:231–238

Yi XS, Yu SL, Shi WX, Sun N, Jin LM, Wang S, Zhang B, Ma C, Sun LP (2011) The influence of important factors on ultrafiltration of oil/water emulsion using PVDF membrane modified by nano-sized TiO2/Al2O3. Desalination 281:179–184

Yu H-D, Tee SY, Han M-Y (2013) Preparation of porosity-controlled calcium carbonate by thermal decomposition of volume content-variable calcium carboxylate derivatives. Chem Commun 49: 4229–4231

Yu H, Cao Y, Kang G, Liu J, Li M, Yuan Q (2009) Enhancing antifouling property of polysulfone ultrafiltration membrane by grafting zwitterionic copolymer via UV-initiated polymerization. J Membr Sci 342:6–13

Zhang Y, Shan X, Jin Z, Wang Y (2011) Synthesis of sulfated Y-doped zirconia particles and effect on properties of polysulfone membranes for treatment of wastewater containing oil. J Hazard Mater 192:559–567

Zhang Y, Liu F, Lu Y, Zhao L, Song L (2013) Investigation of phosphorylated TiO2–SiO2 particles/polysulfone composite membrane for wastewater treatment. Desalination 324:118–126

Zhao S, Wang Z, Wang J, Yang S, Wang S (2011a) PSf/PANI nanocomposite membrane prepared by in situ blending of PSf and PANI/NMP. J Membr Sci 376:83–95

Zhao S, Wang Z, Wei X, Zhao B, Wang J, Yang S, Wang S (2011b) Performance improvement of polysulfone ultrafiltration membrane using PANiEB as both pore forming agent and hydrophilic modifier. J Membr Sci 385:251–262

Zhi S-H, Wan L-S, Xu Z-K (2014) Poly(vinylidene fluoride)/poly(acrylic acid)/calcium carbonate composite membranes via mineralization. J Membr Sci 454:144–154